



Phonon drag thermal Hall effect in metallic strontium titanate

Shan Jiang^a, Xiaokang Li^{a,1}, Benoît Fauqué^b, and Kamran Behnia^{a,2}

Edited by Zachary Fisk, University of California, Irvine, CA; received February 3, 2022; accepted July 18, 2022

SrTiO_3 , a quantum paraelectric, displays a detectable phonon thermal Hall effect (THE). Here, we show that the amplitude of the THE is extremely sensitive to stoichiometry. It drastically decreases upon substitution of a tiny fraction of Sr atoms with Ca, which stabilizes the ferroelectric order. It drastically increases by an even lower density of oxygen vacancies, which turn the system to a dilute metal. The enhancement in the metallic state exceeds by far the sum of the electronic and the phononic contributions. We explain this observation as an outcome of three features: 1) Heat is mostly transported by phonons; 2) the electronic Hall angle is extremely large; and 3) there is substantial momentum exchange between electrons and phonons. Starting from Herring's picture of phonon drag, we arrive to a quantitative account of the enhanced THE. Thus, phonon drag, hitherto detected as an amplifier of thermoelectric coefficients, can generate a purely thermal transverse response in a dilute metal with a large Hall angle. Our results reveal a hitherto-unknown consequence of momentum-conserving collisions between electrons and phonons.

quantum paraelectric | thermal Hall effect | dilute metal | Hall angle | phonon drag

The observation of the thermal Hall effect (THE) in a variety of insulators (1–7) has attracted much recent attention. A transverse thermal gradient produced by a longitudinal flow of neutral carriers of heat requires a microscopic mechanism other than the Lorentz force. In strontium titanate, a nonmagnetic insulator (8), the phononic origin of the THE (5, 9), is uncontested. Theoretical scenarios (10–16) have been proposed to explain how phonons can generate a transverse thermal gradient on top of the longitudinal one.

Ferroelectric transition is aborted by quantum critical fluctuations (17) in strontium titanate. The ground state of this quantum paraelectric (18) is unusually sensitive to the presence of extrinsic atoms (19–21). $\text{Sr}_{1-x}\text{Ca}_x\text{TiO}_3$ is ferroelectric for $x > 0.002$ (19, 22). Introducing a tiny amount of oxygen vacancies, on the other hand, makes the system metallic. With a carrier density of the order of 10^{17}cm^{-3} , $\text{SrTiO}_{3-\delta}$ is a dilute metal with a sharp Fermi surface and a superconducting ground state (23). Double substitution leads to $\text{Sr}_{1-x}\text{Ca}_x\text{TiO}_{3-\delta}$, a polar metal (24, 25), where superconductivity is boosted (26). Here, we present a study of the THE in Ca-substituted (insulating) and in oxygen-reduced (metallic) samples of strontium titanate. We find that the amplitude of the signal is significantly modified in both cases, but in opposite directions. In the case of Ca substitution, we find that the THE is drastically reduced, confirming that stabilization of the ferroelectric order is detrimental to the THE (9). On the other hand, in $\text{SrTiO}_{3-\delta}$, the amplitude of the THE not only exceeds what is found in the undoped insulator, but is also much larger than the sum of the expected electronic contribution and the phononic one. We argue that this surprising result can be understood by invoking the drag (27, 28) between electrons and phonons. In our temperature range of interest, heat is almost exclusively carried by phonons ($\kappa^{ph} \gg \kappa^e$) in this dilute metal. On the other hand, the phonon Hall angle is small ($\kappa_{xy}^{ph} < 10^{-3}\kappa_{xx}^{ph}$), but not the electronic Hall angle, which exceeds unity ($\sigma_{xy} > \sigma_{xx}$ at $\approx 2T$). In this context, momentum-conserving collisions between electrons and phonons can generate a transverse temperature gradient because longitudinal momentum transferred to the electron bath will have a transverse counterpart, which ultimately generates a transverse energy flow. Starting from Herring's picture of phonon drag (27), we will show that this scenario yields a quantitative account of our experimental result.

Such a conclusion implies that phonon drag, hitherto known as an amplifier of the thermoelectric response (29), can have a purely thermal signature, mostly in the transverse channel. In this context, our result identifies a previously unknown consequence of quasi-particle hydrodynamics (30). Momentum-conserving collisions between phonons and electrons (31) are a subject of growing interest in strongly coupled electron–phonon systems (32, 33). Momentum-conserving phonon–phonon collisions are also known to play a role in setting the amplitude of longitudinal thermal conductivity in Callaway's model (34).

Significance

We find that the amplitude of the thermal Hall effect (THE) in strontium titanate drastically varies with atomic substitution. It is suppressed when Sr is substituted by Ca, pointing to the role of ferroelectric fluctuations in generating THE. It is amplified by removing oxygen atoms and the emergence of dilute metallicity. In the latter case, we identify a source of the THE, which is phonon drag in the context of an exceptionally large electronic Hall angle.

Author affiliations: ^aLaboratoire de Physique et d'Étude des Matériaux, Ecole Supérieure de la Physique et de la Chimie Industrielles (ESPCI) Paris–CNRS–Sorbonne Université, PSL University, 75005 Paris, France; and ^bJeunes Equipes de l'Institut de Physique (JEIP), Unité de Service et de Recherche (USR) 3573 CNRS, Collège de France, Paris Sciences et Lettres (PSL) University, 75231 Paris Cedex 05, France

Author contributions: K.B. conceived the study; S.J. and B.F. performed experiments; S.J., X.L., B.F., and K.B. analyzed data; S.J., X.L., B.F., and K.B. participated in the discussion; and S.J. and K.B. wrote the manuscript with input from X.L. and B.F.

The authors declare no competing interest.

This article is a PNAS Direct Submission.

Copyright © 2022 the Author(s). Published by PNAS. This article is distributed under [Creative Commons Attribution-NonCommercial-NoDerivatives License 4.0 \(CC BY-NC-ND\)](https://creativecommons.org/licenses/by-nc-nd/4.0/).

¹Present address: Wuhan National High Magnetic Field Center and School of Physics, Huazhong University of Science and Technology, Wuhan 430074, China.

²To whom correspondence may be addressed. Email: kamran.behnia@espci.fr.

This article contains supporting information online at <https://www.pnas.org/lookup/suppl/doi:10.1073/pnas.2201975119/-/DCSupplemental>.

Published August 22, 2022.

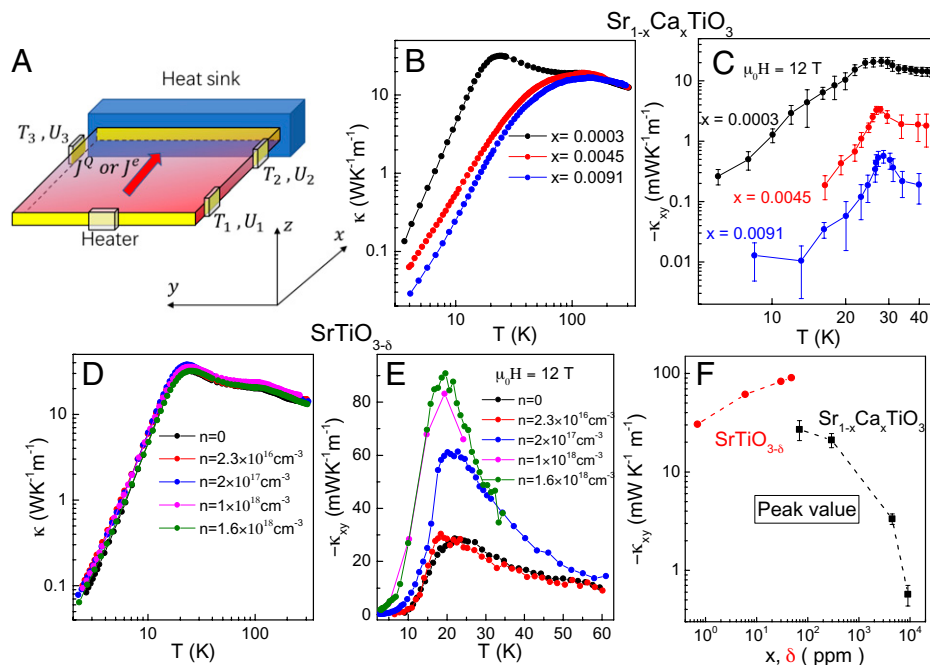


Fig. 1. Evolution of longitudinal and transverse thermal conductivity with Ca substitution and oxygen reduction. (A) Setup for measuring longitudinal and transverse thermal, thermoelectric, and electric coefficients (the yellow pads are gold electrodes). We measured three local temperatures, T_1 , T_2 , and T_3 , and three local voltages, U_1 , U_2 , and U_3 . This allowed us to measure longitudinal and transverse temperature gradients and electric fields caused by a longitudinal heat (J^Q) or electric (J^e) current. (B and C) Temperature dependence of the longitudinal, κ_{xx} (B), and transverse, κ_{xy} (C), thermal conductivity in $\text{Sr}_{1-x}\text{Ca}_x\text{TiO}_3$. The 20 K peak in κ_{xx} is wiped out. κ_{xy} decreases by almost two orders of magnitude. (D) Temperature dependence of κ_{xx} in $\text{SrTiO}_{3-\delta}$, almost unaffected by doping. (E) Temperature dependence of κ_{xy} in $\text{SrTiO}_{3-\delta}$. The amplitude enhances with oxygen substitution. (F) Amplitude of κ_{xy} peak as a function of concentration of Ca atoms (x) and O vacancies (δ) in parts per million (ppm).

Results

Our setup (Fig. 1A) was designed to determine the electric, thermoelectric, and thermal transport coefficients of a single crystal during a single run. In insulating Ca-doped SrTiO_3 single crystals, we measured longitudinal and transverse thermal conductivities. The heat leak through the wires connected to the sample, the heater, and the thermometers is 2 orders of magnitude smaller than the heat current generated by the heater and passing through the sample. In the case of metallic $\text{SrTiO}_{3-\delta}$ single crystals, we measured longitudinal and transverse conductivities in thermal and electric channels, as well as the Seebeck and the Nernst coefficients. In the latter case, by performing two sets of experiments, one with a zero electrical current and another with a zero thermal current, we checked that the transport coefficients respect Onsager reciprocity, as discussed in *SI Appendix*.

Calcium Substitution. The evolution of longitudinal and transverse thermal conductivity with Ca substitution is shown in Fig. 1B and C. One can clearly see that both are affected by Ca substitution. The decrease in κ_{xx} can be attributed to the random distribution of Ca atoms that introduce additional scattering. As in the case of Nb substitution (35), introducing less than a percent concentration of extrinsic atoms is sufficient to wipe out the 20 K peak of the thermal conductivity. The decrease in κ_{xy} is even more drastic. Substituting a tiny fraction ($x = 0.002$) of Sr atoms with Ca is sufficient for stabilizing a long-range ferroelectric order (19). This substitution eventually leads to a 50-fold decrease in the magnitude of κ_{xy} .

A previous study on the effect of ^{18}O substitution on the THE in strontium titanate (9) found a decrease of comparable magnitude. Substituting Sr by Ca (24, 26) and substituting ^{16}O with ^{18}O (21, 36), both stabilize the ferroelectric order, modify the superconducting dome, and generate a polar metal. In both

cases, the large κ_{xy} of the quantum paraelectric solid is drastically suppressed with the stabilization of the ferroelectric order. This suggests a link between the amplitude of κ_{xy} and the presence of ferroelectric fluctuations (11). Note that in ^{18}O -enriched strontium titanate (9), most ^{16}O atoms were substituted, and the 20 K peak in κ_{xx} is still present, in contrast to what is seen here. Yet, κ_{xy} was similarly damped, ruling out that κ_{xy} is simply more sensitive to disorder.

Oxygen Reduction. We investigated the effect of oxygen vacancies on the THE by studying thermal transport in $\text{SrTiO}_{3-\delta}$. Fig. 1B and E shows how the temperature dependence of longitudinal and transverse thermal conductivity in $\text{SrTiO}_{3-\delta}$. The magnitude of longitudinal κ_{xx} barely changes with oxygen reduction. Assuming that each vacancy introduces two electrons, the concentration of vacancies for $n = 1.6 \times 10^{18} \text{cm}^{-3}$ (determined by measuring its Hall resistivity) is only $\delta = 4.8 \times 10^{-5}$ per formula unit, much lower than the lowest amount of Ca substitution ($x = 4.5 \times 10^{-3}$). By measuring the electric conductivity and using the Wiedemann–Franz (WF) law, we estimated that the amplitude of the electronic heat conductivity, κ^e , remains less than 10^{-2} of the total thermal conductivity. Therefore, thermal conductivity near the peak is not significantly reduced by disorder or enhanced by the addition of a finite electronic contribution. In contrast, κ_{xy} significantly increases with increasing n . Let us compare this enhancement with the expected electronic contribution.

Fig. 2A compares the field dependence of κ_{xy} in different samples at 20 K (i.e., near its peak). In the sample with the lowest carrier concentration ($n = 2.3 \times 10^{16} \text{cm}^{-3}$), the amplitude of κ_{xy} is almost identical to the insulating sample and remains linear in magnetic field. In samples with higher carrier concentration, the amplitude of κ_{xy} is larger and shows a gradual trend toward high-field saturation. Fig. 2B shows the electronic contribution

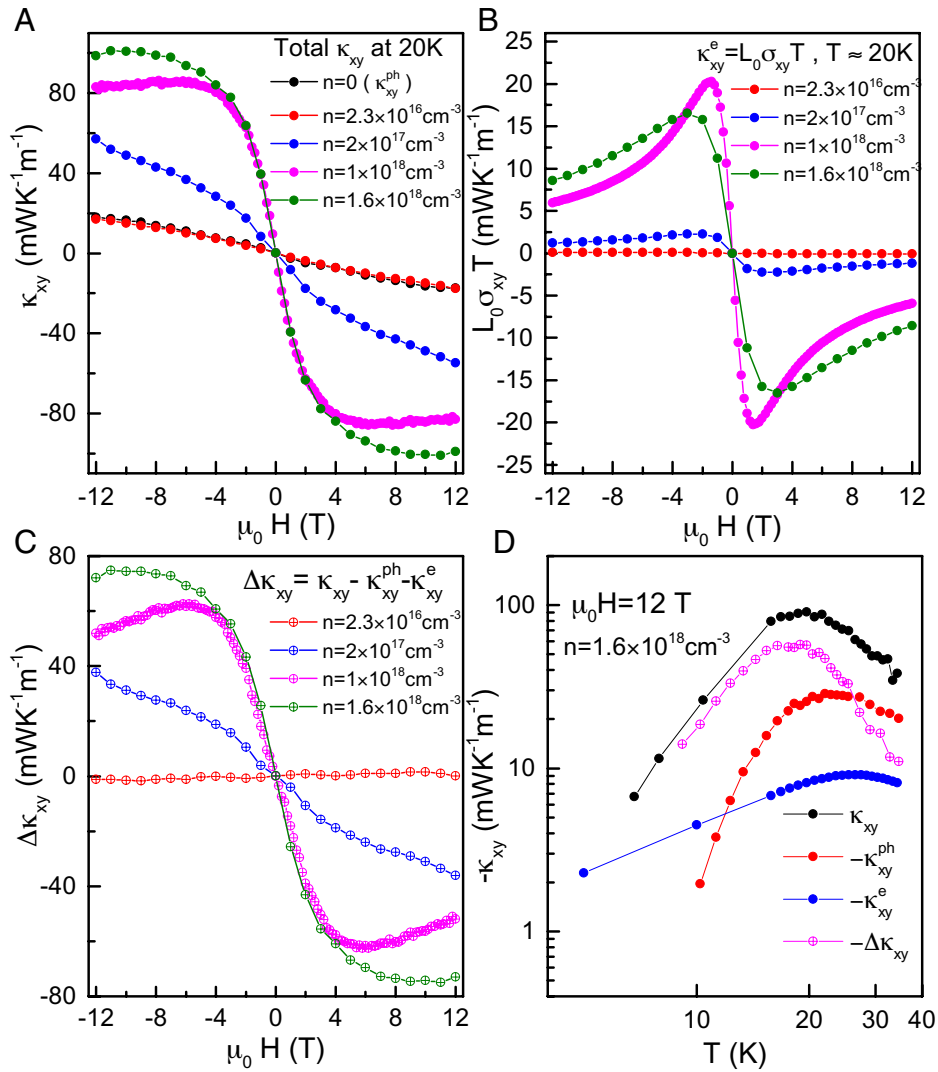


Fig. 2. Three components of the THE in SrTiO_{3-δ}. (A) κ_{xy} as a function of magnetic field in samples with different carrier densities at 20 K. With growing metallicity, the amplitude of κ_{xy} increases, and its field dependence becomes less linear. (B) Field dependence of the electrical Hall conductivity, σ_{xy} , multiplied by $L_0 = \frac{\pi^2 k_B^2}{3e^2}$, and the temperature, T , in the metallic samples. (C) Field dependence of the differential $\Delta\kappa_{xy} = \kappa_{xy} - \kappa_{xy}^{ph} - \kappa_{xy}^e$, which signals the presence of a third term, in addition to the purely electronic and the purely phononic terms. (D) The evolution of κ_{xy} and its three components as a function of temperature. Below 25 K, $\Delta\kappa_{xy}$ is the largest component.

to the THE (estimated from the measured electric Hall conductivity of the metallic samples: $\kappa_{xy}^e = L_0\sigma_{xy}T$). It shows a field-induced saturation similar to what is observed in κ_{xy} . However, subtracting the purely phononic component (taken to be equal to what is observed in the insulator) and the purely electronic component (estimated from the WF law) from the total κ_{xy} leaves us with an additional $\Delta\kappa_{xy} = \kappa_{xy} - \kappa_{xy}^{ph} - \kappa_{xy}^e$. Fig. 2D shows the temperature dependence of the different components of the THE in the sample with the highest carrier concentration ($n = 1.6 \times 10^{18} \text{ cm}^{-3}$). One can see that $\Delta\kappa_{xy}$ exceeds κ_{xy}^{ph} and is several times larger than κ_{xy}^e in most of the temperature range. Note also that the temperature dependence of $\Delta\kappa_{xy}$ is significantly different from κ_{xy}^e .

We shall keep in mind that, at finite temperature, the WF law is not strictly valid. However, the finite-temperature correction does not modify the order of magnitude of the expected electronic thermal conductivity. Moreover, since inelastic scattering damps thermal transport more than the electrical transport, the expected correction to the Lorenz ratio is downward. In copper, such a downward deviation have been observed in the transverse channel

of heat and charge transport, as well as in the longitudinal ones (37). Thus, $L_0\sigma_{xy}T$ gives an upper bound to the expected κ_{xy}^e , and we can safely conclude that enhanced THE is not simply due to the introduction of mobile electrons.

The Thermoelectric Correction to the Thermal Conductivity.

Before discussing the origin of this additional component, we need to distinguish between two thermal conductivities (38). The first one is defined by the Fourier equation:

$$\vec{J}^Q = -\bar{\kappa}\vec{\nabla}T. \quad [1]$$

In the presence of thermoelectric phenomena, the transport equations become:

$$\vec{J}^e = \bar{\sigma}\vec{E} - \bar{\alpha}\vec{\nabla}T, \quad [2]$$

$$\vec{J}^Q = \bar{\alpha}T\vec{E} - \bar{\kappa}'\vec{\nabla}T, \quad [3]$$

where $\bar{\sigma}$ and $\bar{\alpha}$ are the electric and thermoelectric conductivity tensors. Now, if the charge current is kept equal to zero ($\vec{J}^e = \vec{0}$), the combination of the two equations would yield:

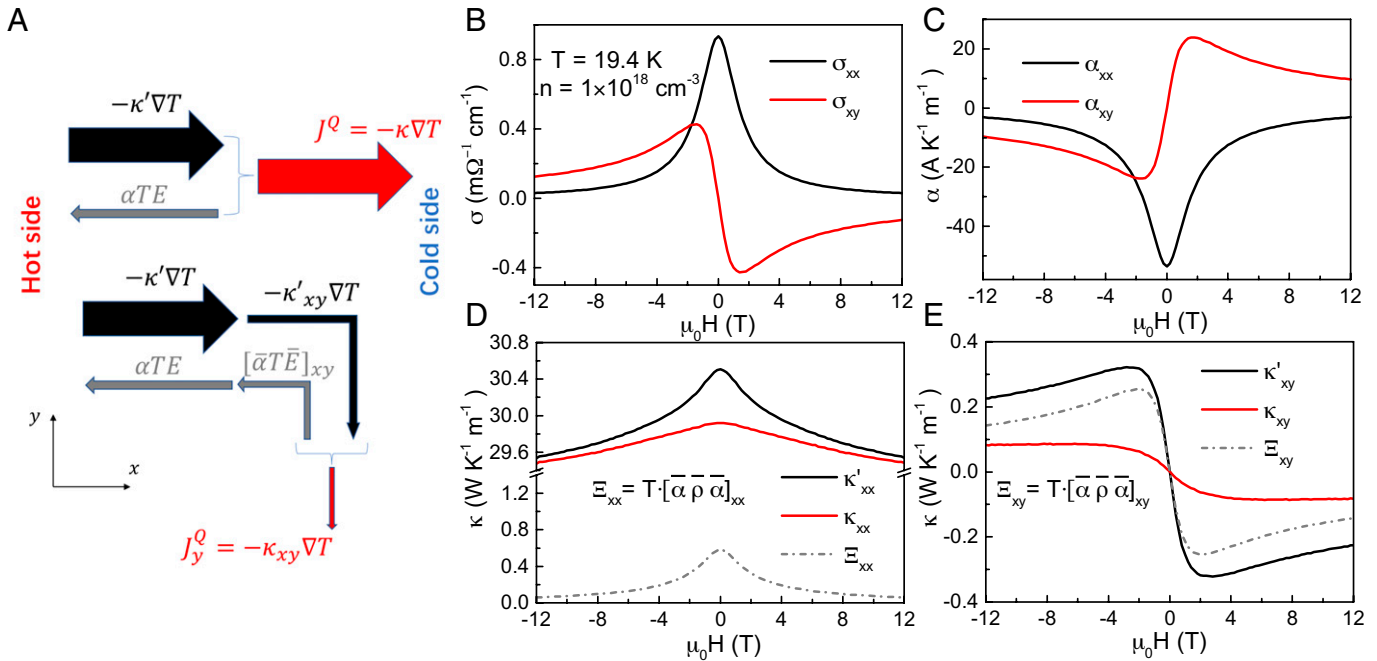


Fig. 3. The two components of heat flux. (A) The heat current density, \vec{J}^Q , consists of two terms in both longitudinal and transverse channels. The first component ($-\bar{\kappa}'\nabla T$) represents the flow of entropy without particle flow. The second ($\bar{\alpha}T$) is the flow of entropy thanks to particle flow. The difference between $\bar{\kappa}$ and $\bar{\kappa}'$ is significant when the second term is not negligible. In our case, this happens for the transverse channel. The width of arrows schematizes the weight of different components. (B) The longitudinal and the transverse electric conductivity as a function of field at 20 K for SrTiO_{3-δ} ($n = 1 \times 10^{18} \text{ cm}^{-3}$). (C) Same for longitudinal and transverse thermoelectric conductivity. $\bar{\alpha} = \bar{\sigma}\bar{S}$. Note that the off-diagonal components rapidly become as large as the diagonal components. (D) $\bar{\kappa}_{xx}$ and $\bar{\kappa}'_{xx}$ as functions of magnetic field. The difference is small. (E) $\bar{\kappa}_{xy}$ and $\bar{\kappa}'_{xy}$ as functions of magnetic field. The difference is significant. Also shown are the diagonal and the off-diagonal components of the $\bar{\Xi} = \bar{\alpha}\bar{\rho}\bar{\alpha}T$ tensor, which quantifies the correction.

$$\vec{J}^Q = (\bar{\alpha}\bar{\rho}\bar{\alpha}T - \bar{\kappa}')\nabla T. \quad [4]$$

The resistivity tensor is simply the inverse of the conductivity tensor: $\bar{\rho} = \bar{\sigma}^{-1}$. Note that the true Onsager coefficient is $\bar{\kappa}'$, and not $\bar{\kappa}$. Practically, this distinction matters only when the first term on the right-hand side of Eq. 4 is not negligible compared to the second term, which happens when the thermoelectric figure of merit is sizeable (38).

We have quantified this difference by measuring longitudinal and lateral temperature differences and electric fields in two distinct experiments. In the first, a finite \vec{J}^Q was applied, and the \vec{J}^e was kept equal to zero. In the second, a finite \vec{J}^e was injected without \vec{J}^Q . This led us to quantify the diagonal and off-diagonal components of the two conductivities, $\bar{\kappa}$ and $\bar{\kappa}'$. We also checked that the data respected Onsager reciprocity, which implies a unique thermoelectric tensor in Eqs. 2 and 3 (see *SI Appendix* for details).

We found that the transverse thermal flow (but not the longitudinal one) is drastically affected by the particle-driven flow of entropy represented by the thermoelectric term (Fig. 3A). In other words, $\bar{\kappa}_{xx} \simeq \bar{\kappa}'_{xx}$, but $\bar{\kappa}_{xy}$ and $\bar{\kappa}'_{xy}$ are significantly different. The reason is the large Hall angle in the electric and the thermoelectric response. As seen in Fig. 3B and C, the diagonal and off-diagonal components of $\bar{\sigma}$ and $\bar{\alpha}$ are of the same order of magnitude. In contrast, the diagonal component of the thermal conductivity tensor (Fig. 3D) is orders-of-magnitude larger than the off-diagonal one (Fig. 3E). As a consequence, while the difference between $\bar{\kappa}_{xx}$ and $\bar{\kappa}'_{xx}$ is of the order of percent (Fig. 3D), $\bar{\kappa}'_{xy}$ is two times larger than $\bar{\kappa}_{xy}$ (Fig. 3E).

Thus, the corrected transverse thermal conductivity is larger than the measured one, which is itself larger than the expected one.

The large electric and thermoelectric Hall angles, which led to this correction, are a key ingredient of the solution to this puzzle. Let us now consider the others.

Discussion

The Three Ingredients of the Scenario. Our scenario invokes three different features of lightly doped strontium titanate. The first is that momentum exchange between phonons and electrons is frequent. Since both the Fermi radius and the phonon thermal wavelength (at our temperature range of interest) are much smaller than the width of the Brillouin zone, such collisions are not Umklapp and conserve momentum. The second feature is that heat is mainly carried by phonons (and not by electrons), $\bar{\kappa}_{xx}^e \ll \bar{\kappa}_{xx}^{ph}$; (Fig. 4A). The third is that the Hall angle of electrons exceeds by far the (thermal) Hall angle of phonons. As one can see in Fig. 4B, the phonon thermal Hall angle is 3 orders of magnitude smaller than the electric Hall angle. Lightly doped strontium titanate is a dilute metal with highly mobile carriers. A moderate magnetic field puts the system in the high field limit, where $\mu B \gg 1$ (39). The combination of these three features generates an additional thermal Hall response: The longitudinal energy flow, mostly carried by phonons, is accompanied by a flow of electrons and its unavoidable transverse counterpart, which ends up by triggering a phononic transverse flow.

Momentum exchange between electrons and phonons (in the presence of heat flow and in the absence of charge current) is known as phonon drag (27, 28). It is known to amplify the thermoelectric response, mostly in semiconductors (27), but also in metals (29). In the case of strontium titanate, previous studies (40, 41) have shown that phonon drag causes a peak in the zero-field Seebeck coefficient around ~ 20 K. We confirmed the presence of such a peak in our samples (*SI Appendix*). Let us now

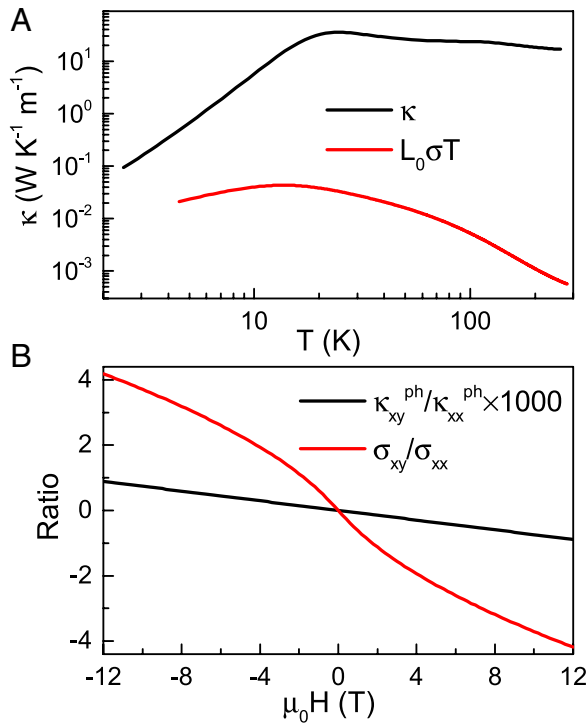


Fig. 4. Longitudinal thermal conductivity and Hall angles. (A) Thermal conductivity (κ_{xx}) of $\text{SrTiO}_{3-\delta}$ ($n = 1 \times 10^{18} \text{cm}^{-3}$) as a function of temperature and its electronic component ($L_0\sigma T$). Phonons are, by far, the dominant carriers of heat. (B) The phonon thermal and the electronic Hall angles as the function of field at $T = 20 \text{K}$. The former is 3 orders of magnitude smaller than the latter.

quantify the expected contribution of phonon drag to transverse thermal transport conductivity.

From Phonon Drag to THE. Phonons streaming from hot to cold exert a drag on the charge carriers. To quantify this effect, Herring (27) considered an equivalent phenomenon: the enhancement in the Peltier coefficient of an isothermal sample caused by the drag exerted on phonons by the electric current. Assuming an approximate proportionality between heat current and crystal momentum, he found that a phonon-drag Peltier effect, Π_{drag} , of either sign can arise:

$$\Pi_{drag} = \pm \frac{m^* v_s^2}{e} f \frac{\tau_p}{\tau_e}. \quad [5]$$

Here, m^* is the effective mass of electrons; v_s is the sound velocity; e is the fundamental charge; τ_p and τ_e are, respectively, the phonon- and the electron-scattering times; and $0 < f < 1$ represents the fraction of collisions suffered by phonons, which leads to momentum exchange between the phonon bath and the electron bath. Using the Kelvin relation, the phonon-drag component of the Seebeck coefficient becomes Π_{drag}/T . To derive Eq. 5, Herring put forward two arguments. First of all, the energy density flux, J^Q , can be approximated by the product of the crystal momentum per unit volume, P , and the square of sound velocity, v_s :

$$J^Q = P v_s^2. \quad [6]$$

The second argument is that the rate at which phonons receive crystal momentum from the electronic carriers is to be balanced with the rate at which they lose it. Therefore:

$$\frac{P}{\tau_p} = \pm f n e E. \quad [7]$$

Here, n is the carrier concentration, and E is the electric field. The loss of crystal momentum out of the phonon bath is countered by what electrons introduce to this bath. The parameter f is a measure of efficiency of momentum flow between the phonon and electron baths. Herring invoked a “hydraulic analogy,” where momentum first flows from electrons to small q phonons, is distributed among phonons, and then is eventually lost. In this analogy f plays the role of a half-open valve. Eq. 5 can be obtained from Eqs. 6 and 7, using the Drude link between the electric field and the electric current ($J^e = \frac{ne^2\tau_e}{m^*} E$).

Let us now consider the twist brought by a large Hall angle to this picture. The Peltier phonon drag implies that an electric current can lead to a phonon energy flow (Fig. 5A). A finite THE driven by phonon drag can be explained in the following way. A finite Nernst–Ettingshausen coefficient implies that a transverse (longitudinal) thermal gradient will generate a longitudinal (transverse) electric current. Then, this electric current, following Herring’s original picture, will generate a thermal current. The latter will be perpendicular to the thermal gradient (Fig. 5B). Therefore, the overall magnitude of this phonon-drag THE will be given by the product of the off-diagonal thermoelectric conductivity, α_{xy} , and Herring’s expression for Peltier phonon drag:

$$\kappa_{xy}(drag) = \alpha_{xy} \frac{m^* v_s^2}{e} f \frac{\tau_p}{\tau_e}. \quad [8]$$

Thus, the component of thermal Hall conductivity generated by mutual drag between electrons and phonons is proportional to the product of α_{xy} , the ratio of phonon- and electron-scattering times $\frac{\tau_p}{\tau_e}$ and the efficiency of momentum transfer between the two baths, parametrized by f . Let us also note the presence of $m v_s^2$. This is the kinetic energy of an electron drifting with the velocity of sound, a less familiar energy scale emerging when electrons and phonons couple to each other (42).

Quantitative Account of the Data. We proceed now to compare $\Delta\kappa_{xy}$ resolved by experiment, with $\kappa_{xy}(drag)$, expected by Eq. 8. With the exception of f , all terms of Eq. 8 are experimentally accessible. The sound velocity is $v_s = 7.8 \text{km/s}$ (43), and the effective mass of electrons is $m^* = 1.8m_e$ (23). τ_p can be extracted

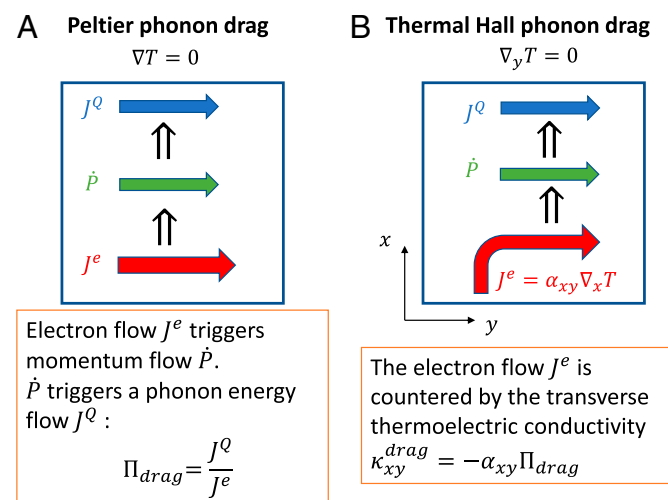


Fig. 5. From phonon drag to thermal Hall conductivity. (A) Herring’s picture of phonon drag in an isothermal sample. Electronic momentum flow generates a phonon momentum flow, which, in turn, leads to a phonon heat flow. The amplitude of this Peltier effect sets the amplitude of the phonon-drag Seebeck effect. (B) Replacing the electronic charge current with a finite transverse thermal gradient multiplied by off-diagonal thermoelectric conductivity quantifies the amplitude of the phonon-drag THE.

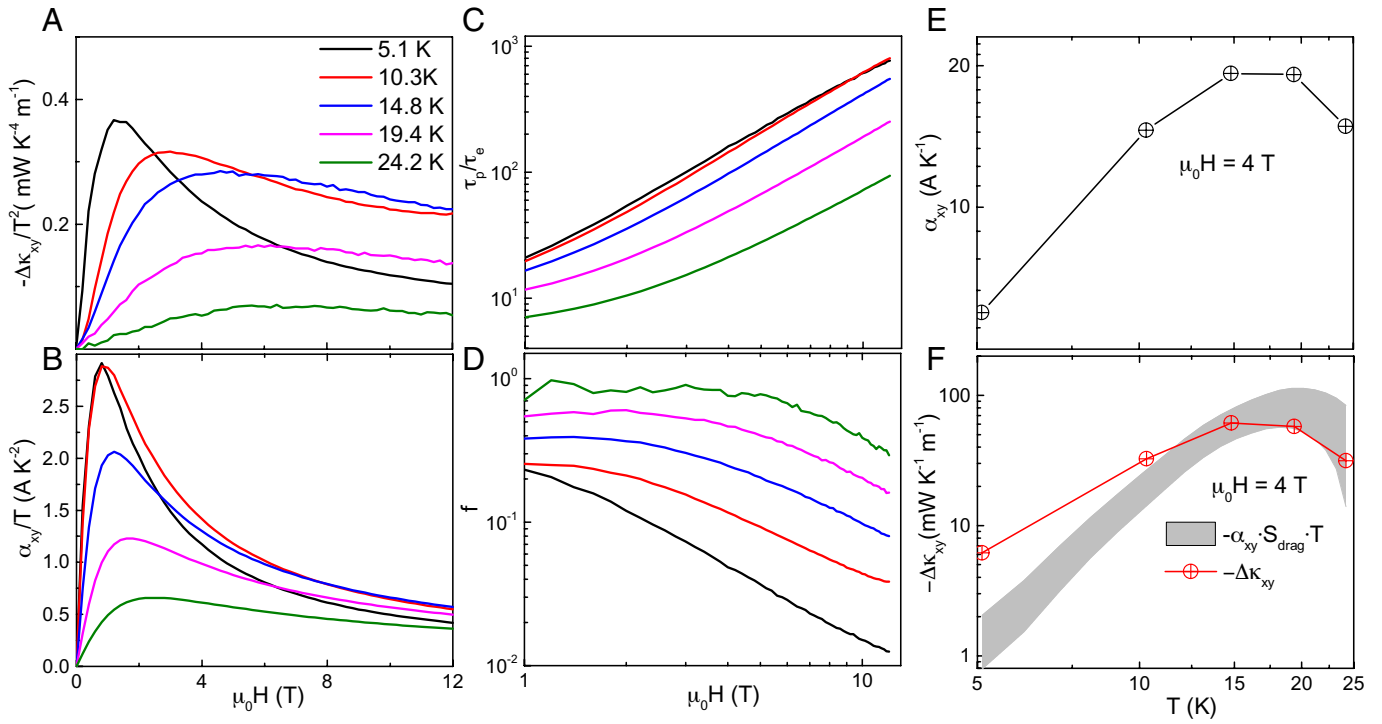


Fig. 6. Quantitative analysis of $\Delta\kappa_{xy}$. (A) Field dependence of $\Delta\kappa_{xy}/T^2$ at different temperatures. (B) Field dependence of α_{xy}/T at different temperatures. In our picture, this is the main driver of the field dependence of $\Delta\kappa_{xy}$. (C) Field dependence of the ratio of the phonon to electron scattering time, extracted from electric and thermal conductivity data. Note that $\tau_p \gg \tau_e$, and the ratio enhances with magnetic field. (D) The field dependence of f , obtained by equating $\Delta\kappa_{xy}$ and $\kappa_{xy}(\text{drag})$, given by Eq. 8. (E) The temperature dependence of α_{xy} at 4 T. (F) The temperature dependence of $-\Delta\kappa_{xy}$ and $-\alpha_{xy}S_{\text{drag}} \cdot T$. The width of the latter represents the uncertainty in separating the phonon drag and the diffusive components of the Seebeck coefficient (SI Appendix).

from phonon thermal conductivity and τ_e from the electrical conductivity.

Fig. 6A shows the nonmonotonous field dependence of $\kappa_{xy}(\text{drag})$, which mirrors the field dependence of α_{xy} (Fig. 6B), which, after an initial increase, steadily decreases in the high-field regime. Since $S_{xx} > S_{xy}$ and $\sigma_{xy} \geq \sigma_{xx}$, $\alpha_{xy} \approx S_{xx}\sigma_{xy}$, and the field dependence of α_{xy} is similar to the field dependence of Hall conductivity, which steadily decreases in the high-field regime ($\sigma_{xy}(B \rightarrow \infty) \rightarrow 0$).

The ratio of τ_p/τ_e , shown in Fig. 6C, is much larger than unity and steadily increases with magnetic field. This is because, as previously documented (39), the mobility of electrons diminishes with magnetic field, presumably because partially extended disorder becomes more effective in scattering electrons with increasing magnetic field, which confines the electron-wave function. The phonon-scattering time, on the other hand, is barely affected by magnetic field.

By assuming equality between $\Delta\kappa_{xy}$ and $\kappa_{xy}(\text{drag})$ and using Eq. 8, we can extract f . The results are shown in Fig. 6D. We find that $f < 1$, attesting to the soundness of our approach. The efficiency of momentum transfer between phonons and electrons is close to one at the peak temperature and steadily decreases with temperature. As the temperature decreases, the relative frequency of electron–phonon-scattering events decreases. We also note that a strong coupling between electrons and soft ferroelectric phonons has been invoked (44, 45) to explain the transport properties of metallic strontium titanate (41, 46). The steady field-induced decrease in f indicates that the efficiency of the momentum transfer between phonons and electrons decreases with the decrease in the electronic scattering time and the growing mismatch between the phonon- and electron-scattering time.

The soundness of our diagnostic can be checked by comparing the extra THE and the phonon-drag Seebeck effect, supposed

to share the same origin. Both effects, measured by distinct experiments, peak around 20 K. Their amplitudes match, too. Eqs. 5 and 8 together with the Kelvin relation ($\Pi = ST$) and the identification of $\Delta\kappa_{xy}$ with $\kappa_{xy}(\text{drag})$ imply an equality between the two extracted quantities: $\Delta\kappa_{xy} \approx -\alpha_{xy}S_{\text{drag}}T$. Fig. 6F compares $\Delta\kappa_{xy}$ and $-\alpha_{xy} \cdot S_{\text{drag}} \cdot T$ as a function of temperature at 4 T. The agreement between 25 K down to 10 K confirms the quantitative self-consistency of the data. The disagreement at 5 K indicates the limits of our approximations when f strongly varies with magnetic field.

Relevance to Other Metallic Solids. Our result implies that the combination of phonon drag (frequently encountered in semiconductors) and a sizeable transverse thermoelectric conductivity, α_{xy} [known to become large when the carrier density is low density and the carrier mobility is high (47)] can give rise to a phonon-drag THE. These conditions can be formulated in term of a hierarchy of time scales. The scattering time of phonons should exceed the scattering time of electrons, and the latter should, in turn, exceed the inverse of the cyclotron frequency, in order to ensure longitudinal-to-transverse conversion. Thus, a sizeable phonon-drag THE requires:

$$\tau_p > \tau_e > \omega_c^{-1}. \quad [9]$$

The second condition is that the rate of momentum lost by phonons is to be comparable to the rate of phonon–electron exchange:

$$f \gg 0. \quad [10]$$

Note that the latter condition can only be satisfied at finite temperature. The hydrodynamic window, identified by Gurzhi (30), requires a hierarchy of time scales, too: The momentum-conserving scattering time should outweigh the boundary-scattering time,

itself larger than the momentum-relaxing scattering time. As a result, hydrodynamic features are expected in a limited temperature window and in a limited number of materials.

Inequalities [9] and [10] specify the conditions for expecting a phonon-drag THE. Long τ_p is expected in a crystal at low temperature when phonon wavelength is long and point defects cannot scatter them. In many dilute metals, when the Bohr radius of the semiconducting parent is long (48), carriers are more mobile than in metallic silicon. As a consequence, the inequality $\tau_e > \omega_c^{-1}$ is easily satisfied at low fields. If electron-phonon momentum exchange happens to be frequent, too, then an effect similar to the one observed here is expected. Possible candidates are Bi₂Se₃ (49), InAs (50), PbTe (51), and their sister compounds. It is not surprising that the THE in metallic cuprates is not detectably amplified by phonon drag (3). In their case, the mobility of carriers in cuprates is low, and, as a consequence, condition [9] is not satisfied. Indeed, the measured Hall angle in La_{1-x}Sr_xCuO₄ is quite small. At $B = 10T$, $\sigma_{xy}/\sigma_{xx} \ll 0.1$ (52), and, therefore, $\omega_c\tau_e < 1$.

The result reported here does not provide a direct solution to the puzzle of phonon THE in insulators. Nevertheless, the complicity between two types of heat carriers, one with a long scattering time (here, phonons) and another with a large Hall angle (here, electrons) may have relevance to other contexts. One can imagine a scenario close to ours in an insulating solid hosting

two types of carriers: ordinary phonons with a long scattering time and magnons or chiral phonons or with a short scattering time and a large transverse response.

Materials and Methods

Samples. SrTiO₃ and Ca-doped SrTiO₃ single crystals were provided by CrysTech and SurfaceNet GmbH. Oxygen-deficient SrTiO₃ samples were obtained by annealing them in a temperature range extending from 700 °C to 1,000 °C under a high vacuum ($< 10^{-6}$ mbar) for 1 to 2 h.

Measurements. We used a one-heater-three-thermometers setup (shown in Fig. 1A) to measure the longitudinal and transverse temperature difference caused by a longitudinal heat current. The thermometers and heater were glued directly on the sample by using silver paste. Five gold electrodes (shown in Fig. 1A) were sputtered on the metallic samples, which were used to measure longitudinal and transverse electric fields.

Data, Materials, and Software Availability. All study data are included in the article and/or supporting information.

ACKNOWLEDGMENTS. This work was supported by the Agence Nationale de la Recherche (ANR-18-CE92-0020-01 and ANR-19-CE30-0014-04), by Jeunes Equipes de l'Institut de Physique du Collège de France, and by a grant attributed by the Ile de France regional council. S.J. acknowledges a grant from the China Scholarship Council.

- K. Sugii *et al.*, Thermal Hall effect in a phonon-glass Ba₃CuSb₂O₉. *Phys. Rev. Lett.* **118**, 145902 (2017).
- Y. Kasahara *et al.*, Unusual thermal Hall effect in a Kitaev spin liquid candidate α -RuCl₃. *Phys. Rev. Lett.* **120**, 217205 (2018).
- G. Grissonnanche *et al.*, Giant thermal Hall conductivity in the pseudogap phase of cuprate superconductors. *Nature* **571**, 376–380 (2019).
- Y. Hirokane, Y. Nii, Y. Tomioka, Y. Onose, Phononic thermal Hall effect in diluted terbium oxides. *Phys. Rev. B* **99**, 134419 (2019).
- X. Li, B. Fauqué, Z. Zhu, K. Behnia, Phonon thermal Hall effect in strontium titanate. *Phys. Rev. Lett.* **124**, 105901 (2020).
- J. A. N. Bruin *et al.*, Robustness of the thermal Hall effect close to half-quantization in a field-induced spin liquid state. *Nat. Phys.* **18**, 401–405 (2022).
- É. Lefrançois *et al.*, Evidence of a phonon Hall effect in the Kitaev spin liquid candidate α -RuCl₃. *Phys. Rev. X* **12**, 021025 (2022).
- C. Collignon, X. Lin, C. W. Rischau, B. Fauqué, K. Behnia, Metallicity and superconductivity in doped strontium titanate. *Annu. Rev. Condens. Matter Phys.* **10**, 25–44 (2019).
- S. Sim *et al.*, Sizable suppression of thermal Hall effect upon isotopic substitution in SrTiO₃. *Phys. Rev. Lett.* **126**, 015901 (2021).
- T. Qin, J. Zhou, J. Shi, Berry curvature and the phonon Hall effect. *Phys. Rev. B Condens. Matter Mater. Phys.* **86**, 104305 (2012).
- J. Y. Chen, S. A. Kivelson, X. Q. Sun, Enhanced thermal Hall effect in nearly ferroelectric insulators. *Phys. Rev. Lett.* **124**, 167601 (2020).
- X. Q. Sun, J. Y. Chen, S. A. Kivelson, Large extrinsic phonon thermal Hall effect from resonant scattering. *arXiv:2109.12117 [v3]* (26 July 2022).
- B. Flebus, A. H. MacDonald, Charged defects and phonon Hall effects in ionic crystals. *Phys. Rev. B* **105**, L220301 (2022).
- H. Guo, S. Sachdev, Extrinsic phonon thermal Hall transport from Hall viscosity. *Phys. Rev. B* **103**, 205115 (2021).
- A. Zabalo, C. E. Dreyer, M. Stengel, Rotational g factors and Lorentz forces of molecules and solids from density-functional perturbation theory. *Phys. Rev. B* **105**, 094305 (2022).
- P. Bhalla, N. Das, Optical phonon contribution to the thermal conductivity of a quantum paraelectric. *J. Phys. Condens. Matter* **33**, 345401 (2021).
- S. E. Rowley *et al.*, Ferroelectric quantum criticality. *Nat. Phys.* **10**, 367–372 (2014).
- K. A. Müller, H. Burkard, SrTiO₃: An intrinsic quantum paraelectric below 4 K. *Phys. Rev. B Condens. Matter* **19**, 3593–3602 (1979).
- J. G. Bednorz, K. A. Müller, Sr_{1-x}Ca_xTiO₃: An XY quantum ferroelectric with transition to randomness. *Phys. Rev. Lett.* **52**, 2289–2292 (1984).
- V. V. Lemanov, E. P. Smirnova, P. P. Szymrikov, E. A. Tarakanov, Phase transitions and glasslike behavior in Sr_{1-x}Ba_xTiO₃. *Phys. Rev. B Condens. Matter* **54**, 3151–3157 (1996).
- M. Itoh *et al.*, Ferroelectricity induced by oxygen isotope exchange in strontium titanate perovskite. *Phys. Rev. Lett.* **82**, 3540–3543 (1999).
- M. A. Carpenter, C. J. Howard, K. Knight, Z. Zhang, Structural relationships and a phase diagram for Sr_{1-x}Ca_xTiO₃ perovskites. *J. Phys. Condens. Matter* **18**, 10725–10749 (2006).
- X. Lin, Z. Zhu, B. Fauqué, K. Behnia, Fermi surface of the most dilute superconductor. *Phys. Rev. X* **3**, 021002 (2013).
- J. Wang *et al.*, Charge transport in a polar metal. *npj Quantum Mater.* **4**, 61 (2019).
- J. Engelmayr *et al.*, Ferroelectric order versus metallicity in Sr_{1-x}Ca_xTiO_{3- δ} ($x = 0.009$). *Phys. Rev. B* **100**, 195121 (2019).
- C. W. Rischau *et al.*, A ferroelectric quantum phase transition inside the superconducting dome of Sr_{1-x}Ca_xTiO_{3- δ} . *Nat. Phys.* **13**, 643–648 (2017).
- C. Herring, Theory of the thermoelectric power of semiconductors. *Phys. Rev.* **96**, 1163–1187 (1954).
- Y. Gurevich, O. Mashkevich, The electron-phonon drag and transport phenomena in semiconductors. *Phys. Rep.* **181**, 327–394 (1989).
- D. K. C. MacDonald, *Thermoelectricity: An Introduction to the Principles* (Dover Publications, Mineola, NY, 2006).
- R. N. Gurzhi, Hydrodynamic effects at low temperature. *Sov. Phys. Usp.* **11**, 255–270 (1968).
- A. Jaoui *et al.*, Formation of an electron-phonon bi-fluid in bulk antimony. *Phys. Rev. X* **12**, 031023 (2022).
- A. Levchenko, J. Schmalian, Transport properties of strongly coupled electron-phonon liquids. *Ann. Phys.* **419**, 168218 (2020).
- X. Huang, A. Lucas, Electron-phonon hydrodynamics. *Phys. Rev. B* **103**, 155128 (2021).
- J. Callaway, Model for lattice thermal conductivity at low temperatures. *Phys. Rev.* **113**, 1046–1051 (1959).
- V. Martelli, J. L. Jiménez, M. Continentino, E. Baggio-Saitovitch, K. Behnia, Thermal transport and phonon hydrodynamics in strontium titanate. *Phys. Rev. Lett.* **120**, 125901 (2018).
- C. W. Rischau *et al.*, Isotope tuning of the superconducting dome of strontium titanate. *Phys. Rev. Lett.* **126**, 013019 (2022).
- Y. Zhang *et al.*, Determining the Wiedemann-Franz ratio from the thermal Hall conductivity: Application to Cu and YBa₂Cu₃O_{6.95}. *Phys. Rev. Lett.* **84**, 2219–2222 (2000).
- K. Behnia, *Fundamentals of Thermoelectricity* (Oxford University Press, Oxford, UK, 2015).
- C. Collignon *et al.*, Quasi-isotropic orbital magnetoresistance in lightly doped SrTiO₃. *Phys. Rev. Mater.* **5**, 065002 (2021).
- T. A. Cain, A. P. Kajdos, S. Stemmer, La-doped SrTiO₃ films with large cryogenic thermoelectric power factors. *Appl. Phys. Lett.* **102**, 182101 (2013).
- C. Collignon, P. Bourges, B. Fauqué, K. Behnia, Heavy nondegenerate electrons in doped strontium titanate. *Phys. Rev. X* **10**, 031025 (2020).
- C. H. Mousatov, S. A. Hartnoll, Phonons, electrons and thermal transport in Planckian high T_c materials. *npj Quantum Mater.* **6**, 81 (2021).
- W. Rehwald, Anomalous ultrasonic attenuation at the 105° K transition in strontium titanate. *Solid State Commun.* **8**, 607–611 (1970).
- A. Kumar, V. I. Yudson, D. L. Maslov, Quasiparticle and nonquasiparticle transport in doped quantum paraelectrics. *Phys. Rev. Lett.* **126**, 076601 (2021).
- K. G. Nazaryan, M. V. Feigel'man, Conductivity and thermoelectric coefficients of doped SrTiO₃ at high temperatures. *Phys. Rev. B* **104**, 115201 (2021).
- X. Lin, B. Fauqué, K. Behnia, T. Scalable, ²resistivity in a small single-component Fermi surface. *Science* **349**, 945–948 (2015).
- K. Behnia, H. Aubin, Nernst effect in metals and superconductors: A review of concepts and experiments. *Rep. Prog. Phys.* **79**, 046502 (2016).
- K. Behnia, On mobility of electrons in a shallow Fermi sea over a rough sea floor. *J. Phys. Condens. Matter* **27**, 375501 (2015).
- B. Fauqué *et al.*, Magneto-thermoelectric properties of Bi₂Se₃. *Phys. Rev. B Condens. Matter Mater. Phys.* **87**, 035133 (2013).
- A. Jaoui *et al.*, Giant Seebeck effect across the field-induced metal-insulator transition of InAs. *npj Quantum Mater.* **5**, 94 (2020).
- Y. I. Ravich, B. A. Efimova, I. A. Smirnov, *Semiconducting Lead Chalcogenides* (Monographs in Semiconductor Physics, Springer US, New York, ed. 1, 1970), vol. 5.
- Y. Ando, Y. Kurita, S. Komiya, S. Ono, K. Segawa, Evolution of the Hall coefficient and the peculiar electronic structure of the cuprate superconductors. *Phys. Rev. Lett.* **92**, 197001 (2004).